Outcrop	Elevation (m)	Height (m)	Facies description	Inferred depositional environment
Fig. 4a	-3680	80	Variably massive, wedged, erosion-resistant facies, and variably toned recessive intervals	Fluvial floodplain
Fig. 3c	-3862	25	Planar bedding and irregular, crosscutting erosion resistant lip	Termination of dune field due to shift to more humid climate
Fig. 3b	-3865	30		
Fig. 2c	-3901	25	Wavy crossbedding	Aeolian dunes (lee-side spurs)
Fig. 2e	-3922	10	Trough crossbedding	Aeolian dunes
Fig. 2d	-3975	20		
Rover	-4095	NA	Murray fm. has primarily finely bedded mudstones*	Lacustrine*

Table S1: Summary with middle elevation and height of outcrops shown on figures 2-4, interpreted structures and related proposed model in elevation order. Sol 2690 rover elevation as reference. *(Edgar et al., 2018, 2020; Fedo et al., 2018). Outcrops exposures were selected at the center steep slopes on large buttes avoiding areas significantly affected by camera perspective (Fig. S9).

Comment on investigation of the proposed model (Table S1): Future ground investigation by the Curiosity rover may test and refine the proposed model with key paleoenvironmental markers. The aeolian stratigraphic architectures of the lower LSu record signals from dune autogenics, e.g., interacting surfaces, dune migration, and allogenic boundary conditions, e.g., changes in wind direction. Boundary conditions and autogenics represent paleoenvironmental conditions at the time of aeolian accumulation, including water table elevation, wind regime, and sediment availability, making the lower LSu stratigraphy, including the marker bed, an important record of the surface environment at Gale crater. Higher up, for the fluvial floodplain environments, observations should focus on the facies analysis of (i) the recessive floodplain deposits to differentiate between their long-lived or ephemeral subaqueous origin abd (ii) the channel sandstone bodies to understand the paleoflow regime, i.e. single or multiple, and if intermittent or long-lived.

Stratigraphic units shown on Figure 1:

While the present manuscript discusses an analysis focused on the layered sulfate-bearing unit (LSu) interval, the column shown on Figure 1 is a thick (~1 km) overview of information on stratigraphic units of Mt Sharp taken from different sources (Table S2).

Unit	**Description**
Murray formation	The stratigraphic column for the Murray formation is sourced after Fedo et al. (2018)
Clay-bearing unit	The upper limit on the clay-bearing interval correspond to the elevation where the planned rover traverse crosses the boundary of unit 2 of the geologic map in Stack et al. (2017). As discussed in their abstract, the unit 2 area is defined based on morphology and texture but also corresponds well to clay mineral signatures observed from orbit.
Sulfate-clay transition	This interval is in between the clay-bearing and the layered sulfate-bearing unit.
Layered Sulfate-bearing unit	The layered sulfate-bearing (LSu) area is defined by Fraeman et al. (2016); the lower limit shown on Fig. 1 is the elevation where the planned rover traverse crosses the boundary.
Yardangs	The yardangs unit, also follows the definition by Fraeman et al. (2016), lies unconformably onto the LSu. The interval of elevations shown on Fig. 1 correspond to the range for the yardangs unit observed on the map.

Table S2: Description of stratigraphic units shown on Figure 1.

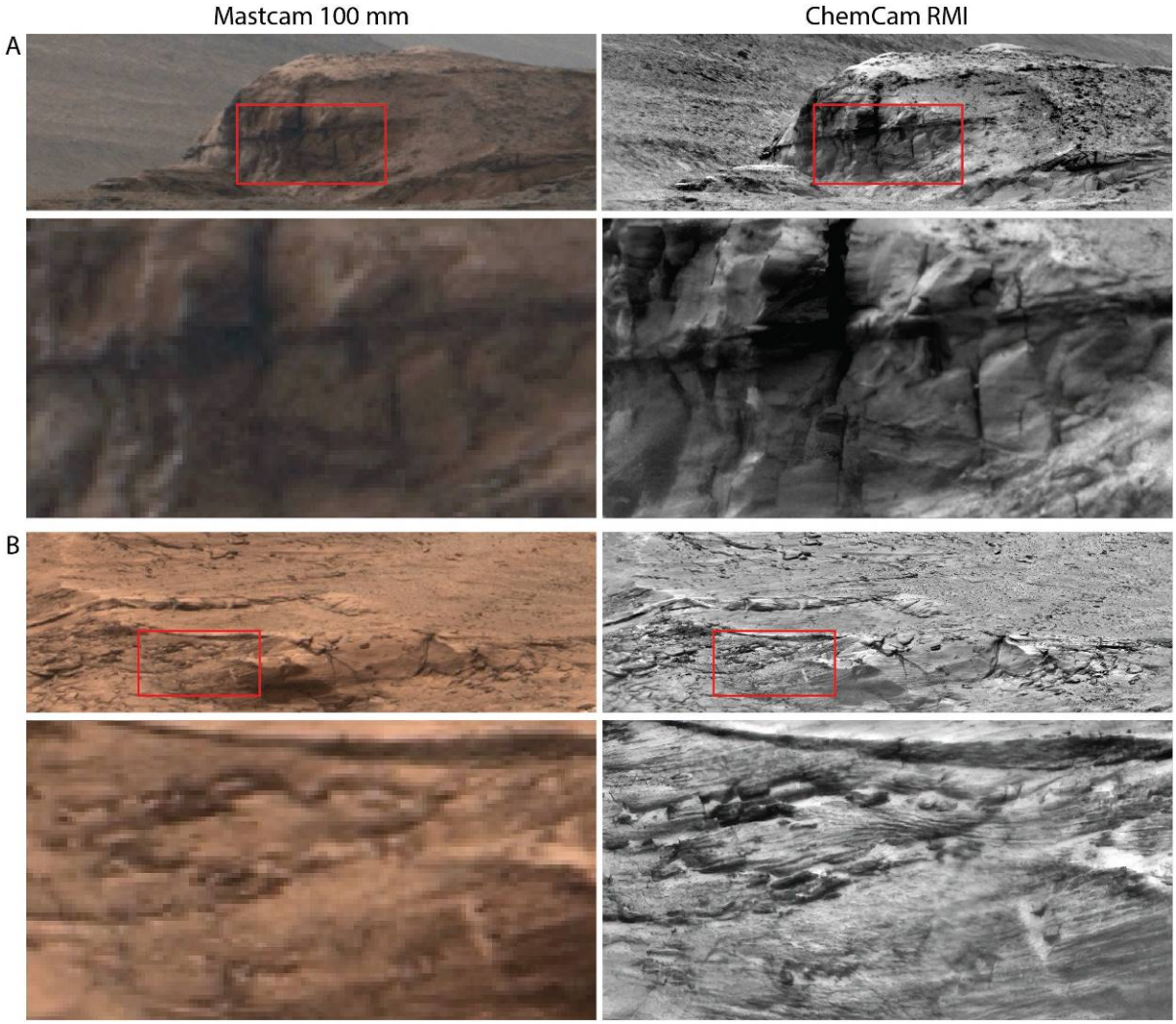

Figure S1: Comparison between Mastcam 100 mm and ChemCam RMI images on two long distance outcrops. **A**, outcrop at 1.7 km distance used in Figure 2e with Mastcam: mcam12158 and RMI: sol 2295, ccam02295. **B**, outcrop at 1.6 km distance used in Figure 2d with Mastcam: mcam12686 and RMI: sol 2396, ccam04395. Additional comparison between the two imagers to highlight the absence of any significant image distortion is found Fig. S8.

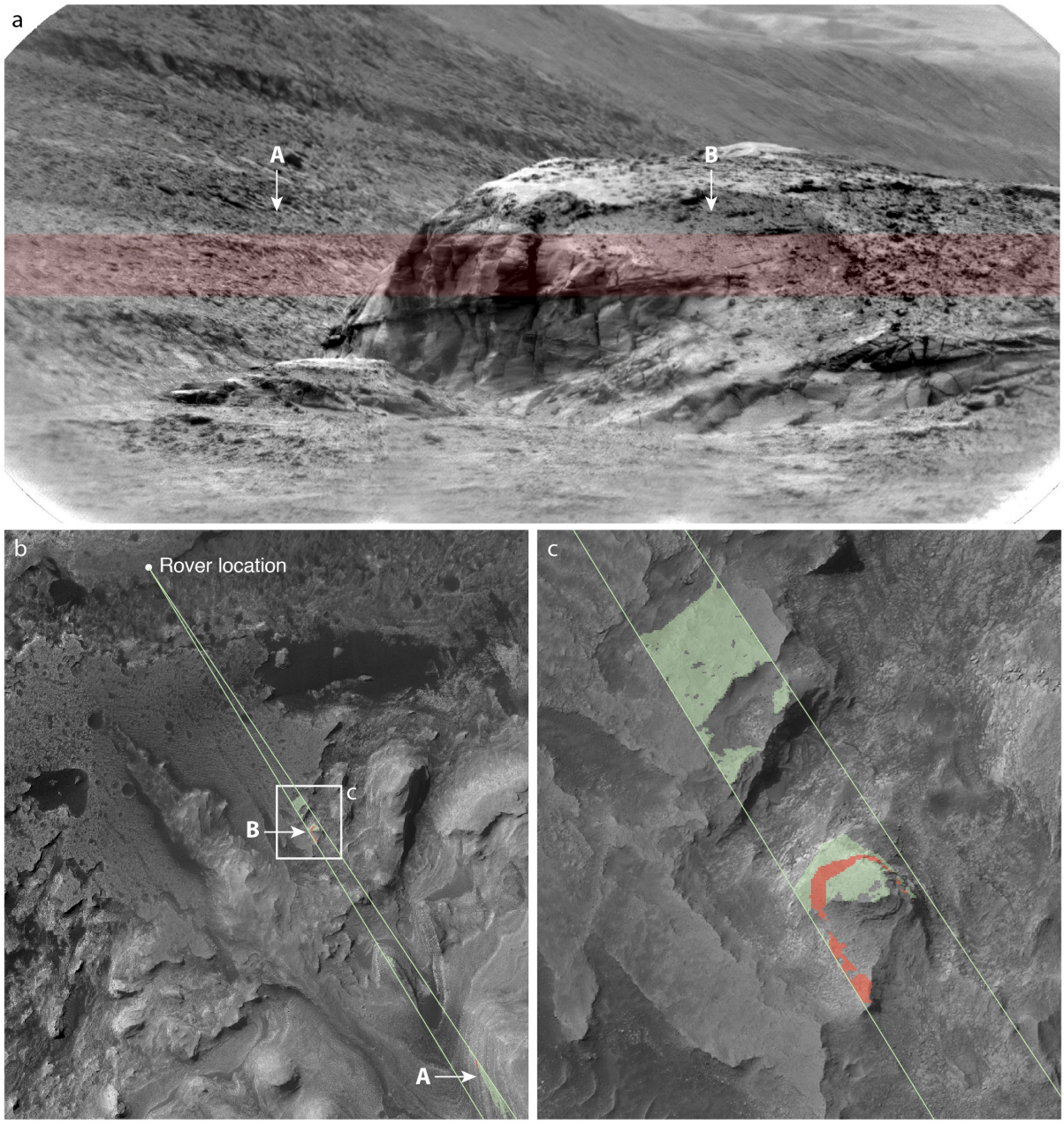

Figure S2: RMI mosaic (**a**, sol 2295 ccam02295, see Fig. 2e) with red band shown to highlight the center viewshed area projected on the HiRISE map (**b**, **c**). These view shed maps and the image help identify the outcrop precisely on the terrain map (shaded green and red area, with green lines representing azimuth boundaries on view angle from rover location), and discriminate between foreground (**B**) and background (**A**).

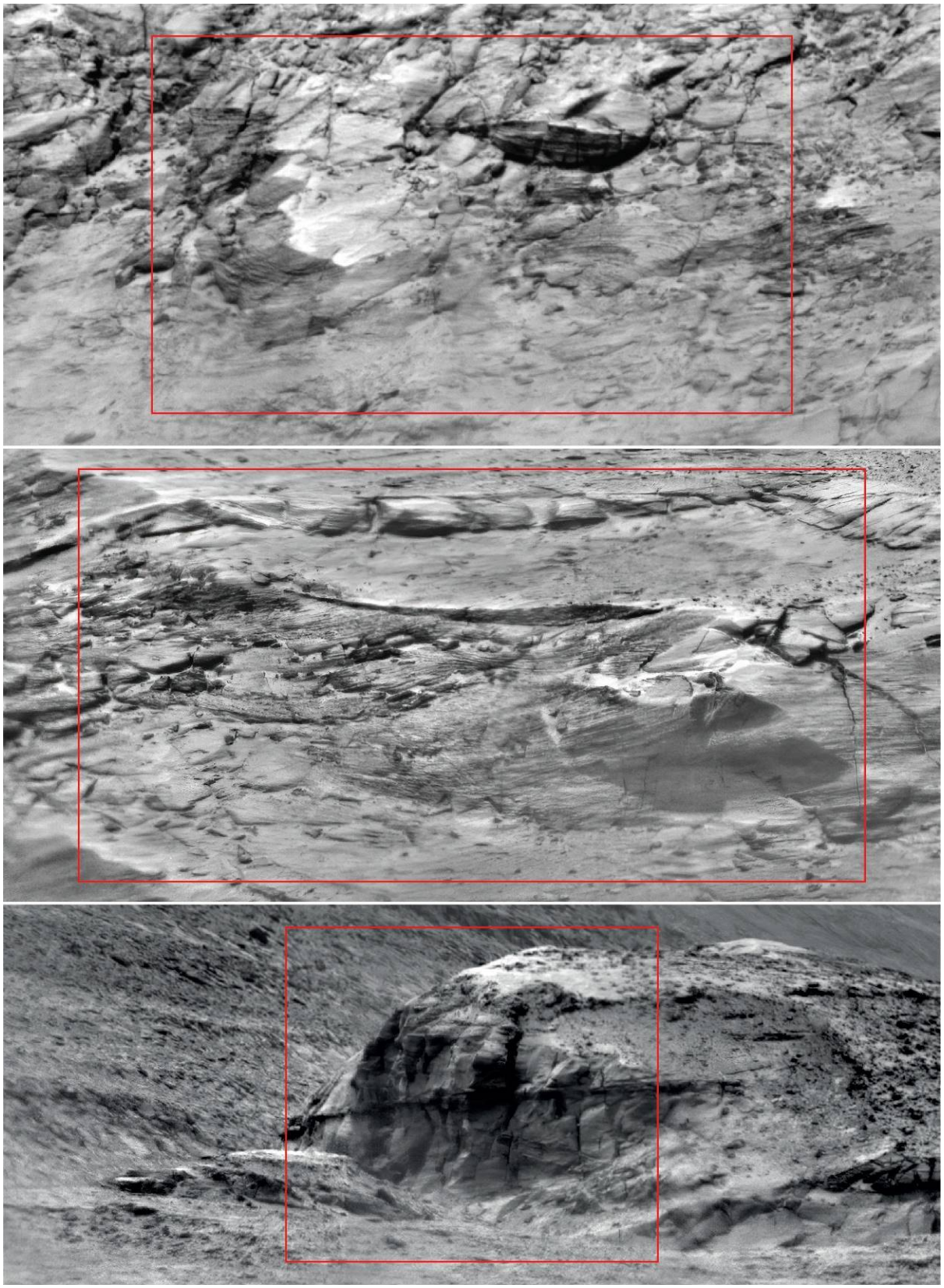

Figure S3 Larger RMI mosaics that provide context for mosaics on Figure 2. Footprints of Figure 2 panels are outlined in red. From top to bottom: Fig. 2c, sol 2435, ccam03435; Fig. 2d, sol 2396, ccam04395; Fig. 2e, sol 2295, ccam02295. Images are all shown at the same spatial resolution as Figure 2.

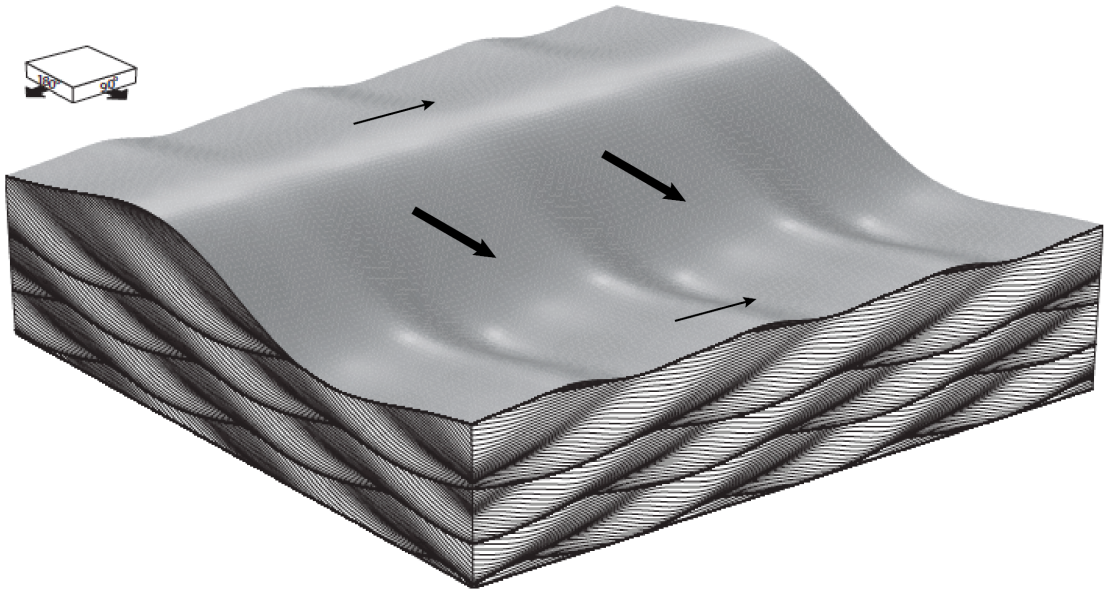

Figure S4: Simulation of sedimentary structures formed by migrating aeolian dunes after Rubin & Carter (1987). This case shows the main dunes migrating in a direction (thick arrow) perpendicular to superimposed smaller dunes (thinner arrows). The resulting crossbedding pattern can be observed on both directions of the vertical cross sections and lacks tabular planar cross beds.

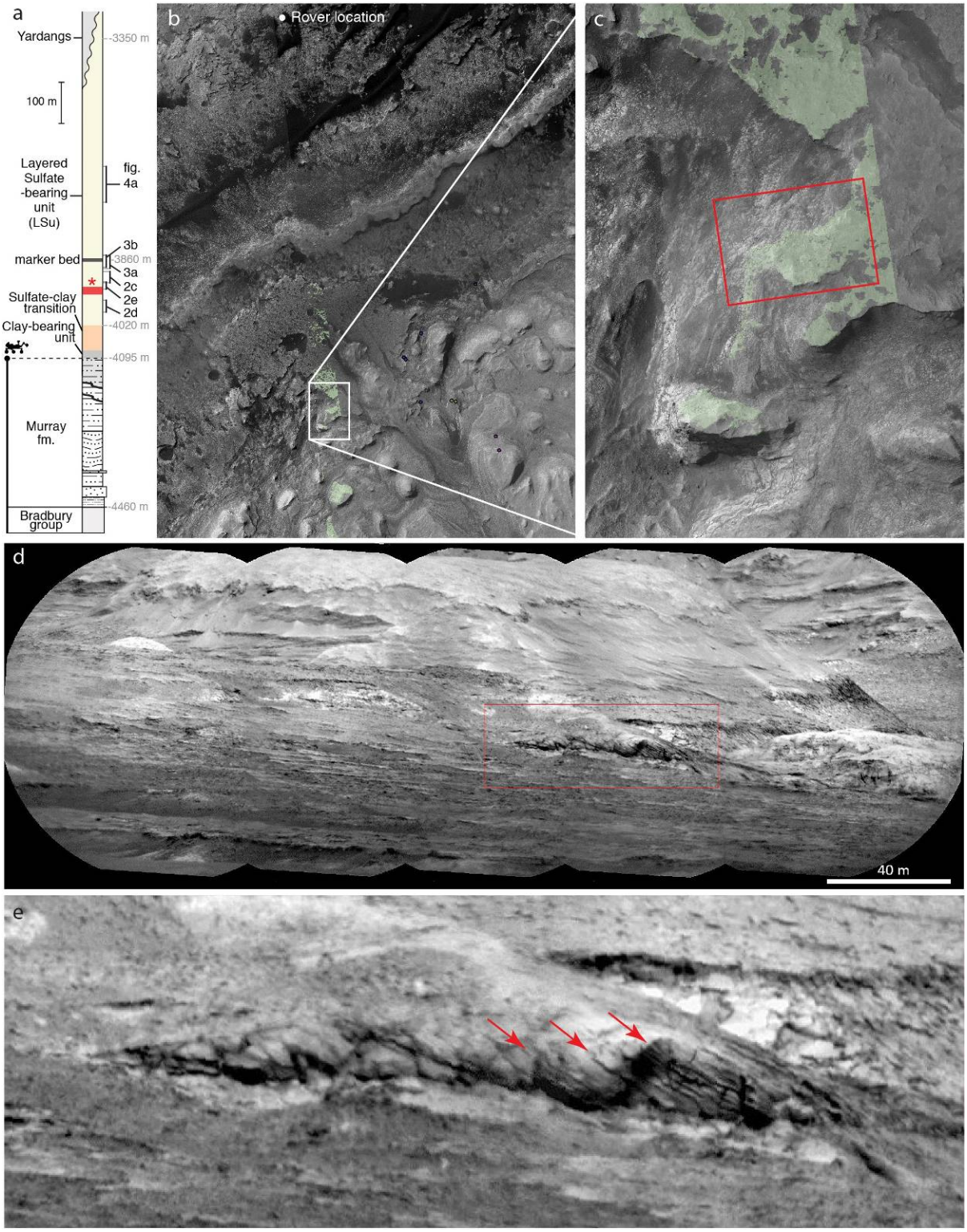

Figure S5: Location of RMI mosaic ccam07239 in the stratigraphy just below the marker bed (**a**; see red star, modified from Fig. 1) and view shed of the RMI mosaic on HiRISE map (**b**, **c**). RMI mosaic (**d**) with highlighted outcrop (**e**; red rectangle) showing structures also consistent with large scale cross-bedding (arrows).

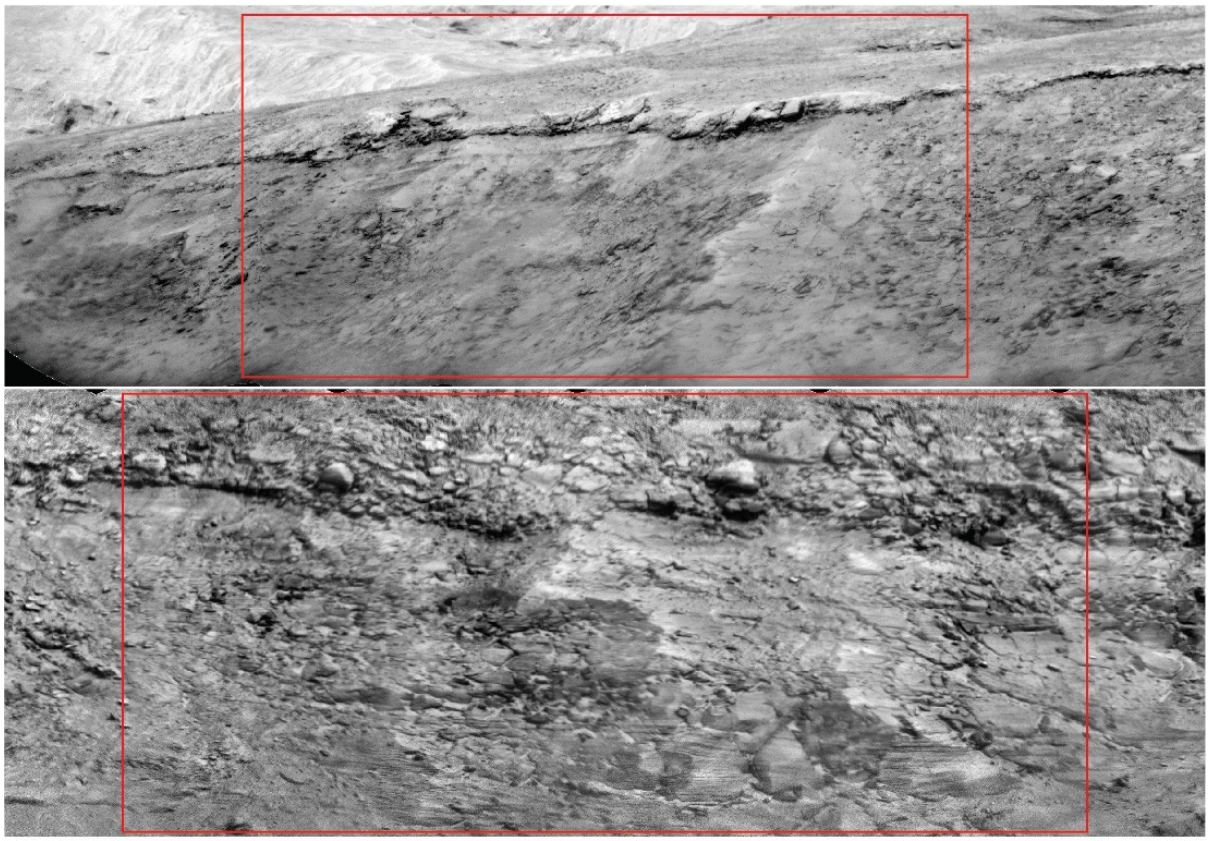

Figure S6 Larger RMI mosaics that provide context for mosaics on Figure 3 with annotated frame (red). From top to bottom: Fig. 3b, sol 2461, ccam04461; Fig. 3c, sol 2852, ccam04851.

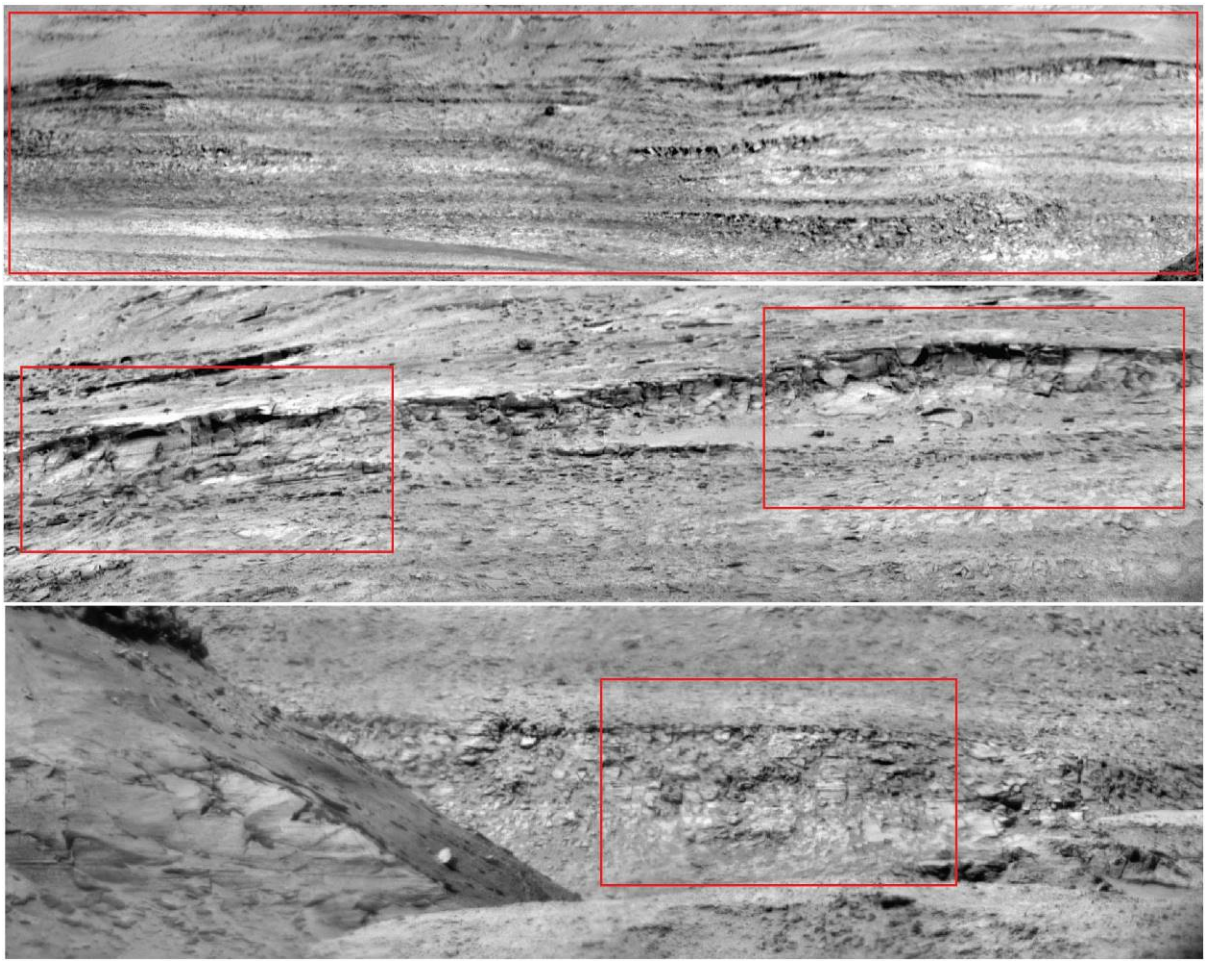

Figure S7 Larger RMI mosaics that provide context for mosaics on Figure 4 with annotated frame (red). From top to bottom: Fig. 3a, sol 1283, ccam02283; Fig. 3b and 3c, sol 1878, ccam04877; Fig. 3d, sol 2640, ccam05640.

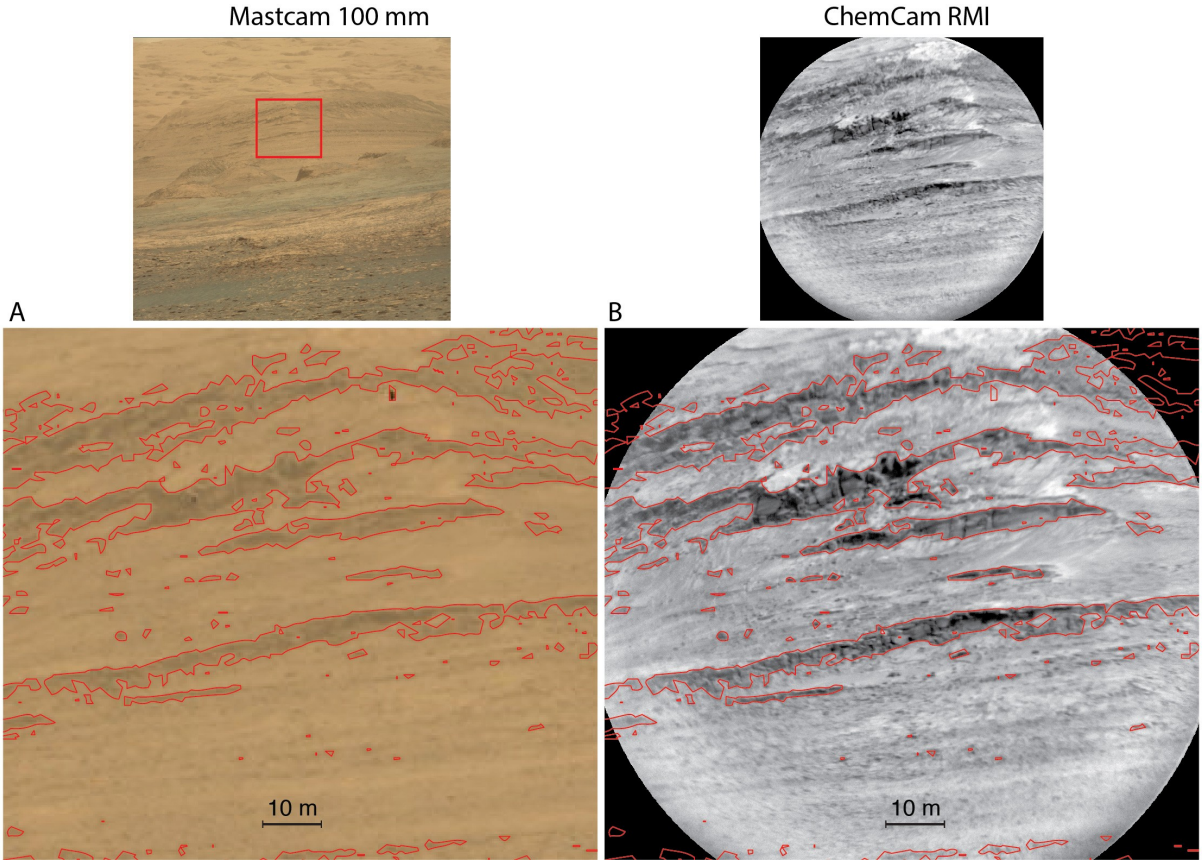

Figure S8 Geometric comparison of Mastcam M100 and ChemCam RMI of the same outcrop features at long distance (6 km). Both individual images are taken from the same location on sol 1628. Edge detection (red contours) was performed on the closeup the Mastcam image to highlight the geometry of shadowed cliffs on the image (**A**). The same contours were copied and pasted over the RMI (**B**) highlighting no significant geometric differences introduced by RMI imaging, at least at the level of detail used for our study. Mosaics are then assembled by translating individual tiles into their best-fit relative positions and blended seamlessly.

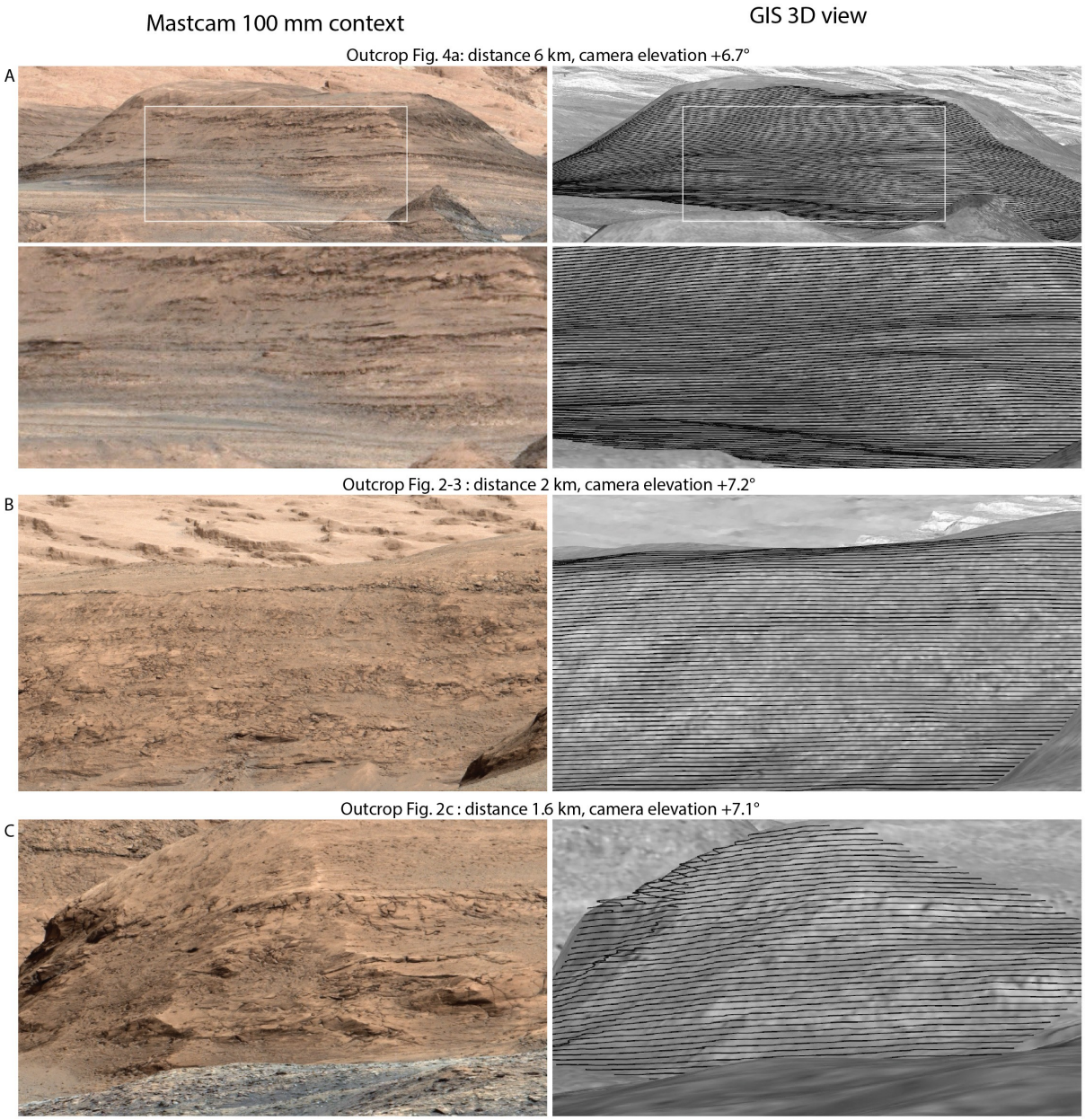

Figure S9: **Left**: Mastcam context of outcrops documented in this study (**A**: mcam06060 for outcrop shown on Fig. 4a, and **B** and **C**: mcam12635 for Fig. 3b, 3c, 2b and 2c). **Right**: Same camera view angle simulated on GIS using HiRISE stereo digital elevation model (DEM) on Gale crater landing site (https://astrogeology.usgs.gov/search/map/Mars/MarsScienceLaboratory/Mosaics/MSL_Gale_DEM_Mosaic_10m), with 1 m accuracy. Localized elevation contours (**A**: 5 m spacing, **B** and **C**: 2 m spacing) are overlaid on the outcrop simulated view as 3D line objects (black lines). They highlight that the outcrop relief, as seen from the camera angle, does not significantly alter observations given the scale of interpreted structures on ChemCam RMIs in this study; contour lines remain mostly parallel on the central area of the outcrops.

Additional references

Edgar, L. A., Gupta, S., Rubin, D. M., Lewis, K. W., Kocurek, G. A., Anderson, R. B., et al. (2018). Shaler: in situ analysis of a fluvial sedimentary deposit on Mars. *Sedimentology*, *65*(1), 96–122. https://doi.org/10.1111/sed.12370

Edgar, L. A., Fedo, C. M., Gupta, S., Banham, S. G., Fraeman, A. A., Grotzinger, J. P., et al. (2020). A Lacustrine Paleoenvironment Recorded at Vera RubinRidge, Gale Crater: Overview of the Sedimentology and Stratigraphy Observed by the Mars ScienceLaboratory Curiosity Rover. *Journal of Geophysical Research: Planets*, *125*(3), e2019JE006307. https://doi.org/10.1029/2019JE006307

Fedo, C., Grotzinger, J. P., Gupta, S., Fraeman, A., Edgar, L., Edgett, K., et al. (2018). Sedimentology and Stratigraphy of the Murray Formation, Gale Crater, Mars (Vol. 49, p. 2078). Presented at the LPSC.

Fraeman, A. A., Ehlmann, B. L., Arvidson, R. E., Edwards, C. S., Grotzinger, J. P., Milliken, R. E., et al. (2016). The stratigraphy and evolution of lower Mount Sharp from spectral, morphological, and thermophysical orbital data sets. *Journal of Geophysical Research: Planets*, *121*(9), 1713–1736.

Rubin, D. M., & Carter, C. L. (1987). *Cross-Bedding, Bedforms, and Paleocurrents*. SEPM (Society for Sedimentary Geology). https://doi.org/10.2110/csp.87.01

Stack, K. M., Cofield, S. M., & Fraeman, A. A. (2017). GEOLOGIC MAP OF THE MSL CURIOSITY ROVER EXTENDED MISSION TRAVERSE OF AEOLIS MONS, GALE CRATER, MARS (p. 1889). Presented at the LPSC 48. Retrieved from https://www.hou.usra.edu/meetings/lpsc2017/pdf/1889.pdf